Journal of Catalysis 281 (2011) 352–360

Contents lists available at ScienceDirect

Journal of Catalysis

journal homepage: www.elsevier.com/locate/jcat

Tuning the support acidity of flame-made $Pd/SiO_2–Al_2O_3$ catalysts for chemoselective hydrogenation

Jun Huang [a,c], Yijiao Jiang [a], Niels van Vegten [a], Michael Hunger [b], Alfons Baiker [a,*]

[a] Institute of Chemical and Bioengineering, Department of Chemistry and Applied Biosciences, ETH Zurich, Hönggerberg, HCI, CH-8093 Zurich, Switzerland
[b] Institute of Chemical Technology, University of Stuttgart, D-70550 Stuttgart, Germany
[c] Laboratory for Catalysis Engineering, School of Chemical and Biomolecular Engineering, The University of Sydney, NSW 2006, Australia

ARTICLE INFO

Article history:
Received 29 March 2011
Revised 19 May 2011
Accepted 20 May 2011
Available online 25 June 2011

Keywords:
Palladium
Silica–alumina
Support acidity
Flame spray pyrolysis
Chemoselective hydrogenation
Acetophenone
Solid-state NMR
DRIFTS

ABSTRACT

Palladium nanoparticles on silica–alumina (Pd/SA) with tunable surface acidity were prepared by single-step flame spray pyrolysis and tested for the chemoselective hydrogenation of acetophenone under solvent-free conditions in a stirred autoclave at 50 bar. Quantitative solid-state NMR spectroscopy of the catalysts with different Si/Al ratio revealed that the concentration of Brønsted acid sites in these catalysts increases with increasing aluminum content up to 70 at%. The support acidity directly influenced the electronic properties of the Pd nanoparticles as proved by DRIFT spectroscopy with CO as probe molecule. Pd/SA with 15 at% aluminum (Pd/SA-15) exhibited excellent chemoselectivity for C=O bond hydrogenation of acetophenone. At 170 °C and 50 bar H_2, acetophenone was converted to ethylbenzene with a selectivity of 99.9%. Beside 0.1% 1-phenylethanol, no other by products were detected. Further enhancement of the support acidity in catalysts with higher Al content resulted in higher reaction rate (TOF) and in additional products originating from the competitive hydrogenation of the aromatic ring.

1. Introduction

Flame spray pyrolysis (FSP) is a single-step method combining synthesis and calcination and is thus promising for the preparation of nanocatalysts. This method can shorten the synthesis time from days to seconds and provide catalytic materials with properties not easy accessible with other synthesis methods [1–5]. Recently, we have used FSP to generate amorphous silica–alumina (SA) with tunable Brønsted acidity [6]. This solid acid can be tuned to offer optimal acidity for efficient catalysis of a particular target reaction. SAs are one type of important acids in oil refinery and biofuel generation [7,8]. Furthermore, SAs are excellent supports for metal nanoparticles in many catalytic applications, such as hydrogenations, oxidations, reforming, and deNOx reactions [8]. The catalytic properties of these catalysts are generally influenced by the support properties. We have shown recently that the acid–base properties of similarly prepared flame-derived Pt/SA catalysts can influence the electronic properties of Pt particles and thereby affect the enantioselectivity and diastereoselectivity in platinum-catalyzed hydrogenations [5,9]. It has been proposed earlier by the group of Koningsberger that basic supports lead to a higher Pt—H bond strength, while the acidic and more covalent supports weaken this bond strength during hydrogenation [10].

Generally, the formation of metal nanoparticles on acidic supports always generates bifunctional catalysts [8]. Addition of acids or acidic supports is often used to enhance the efficiency of catalysts for hydrogenation, hydrogenolysis, and hydrocracking processes [11,12]. Chemoselective hydrogenation of organic compounds containing carbonyl groups is an important reaction not only in organic syntheses of fine chemicals and pharmaceuticals but also in bio-oil upgrading to fuels and high-value chemicals [7,12]. In hydrodeoxygenation of bio-oils, it is desirable to only promote hydrogenolysis of carbonyl groups to saturated C—C bonds and avoiding hydrogenation of aromatic rings because the latter decreases the octane number of the produced fuels and results in undesired hydrogen consumption. The hydrogenation of acetophenone is therefore an ideal test reaction for chemoselective hydrogenation, because it involves competitive hydrogenation of carbonyl and phenyl groups. Furthermore, the selective hydrogenation of acetophenone has practical relevance for the production of phenylethanol for perfumery industry and ethylbenzene for polymer and fuel industry. Various supported Pd, Pt, Ni, Cu, Ti, and Ru catalysts have been employed in the hydrogenation of acetophenone [4,12–15]. The group of Vannice [13] showed that by proper choice of the support, the selectivity to ethylbenzene can be enhanced in the platinum-catalyzed vapor-phase

* Corresponding author. Fax: +41 44 632 11 63.
E-mail address: baiker@chem.ethz.ch (A. Baiker).

0021-9517/$ - see front matter © 2011 Elsevier Inc. All rights reserved.
doi:10.1016/j.jcat.2011.05.023

hydrogenation of acetophenone. $Pt/SiO_2–Al_2O_3$ showed higher selectivity to ethylbenzene than Pt/TiO_2, Pt/SiO_2, and Pt/Al_2O_3. The enhanced selectivity was attributed to phenylethanol dehydration to styrene on the acidic support followed by a hydrogenation step on the platinum. Interestingly, for the palladium-catalyzed hydrogenation of acetophenone, it was found that preadsorbed oxygen on Pd/SiO_2 enhances the selectivity to ethylbenzene compared with corresponding reduced catalysts [14]. Recently, our group reported a green pathway for the chemoselective hydrogenation of acetophenone on ionic liquid-stabilized nanoparticles [15].

Here, we synthesized silica–alumina–supported palladium catalysts by means of single-step flame spray pyrolysis and investigated the effect of changes in the support acidity on the electronic and catalytic properties of the metal nanoparticles. As a powerful method for characterizing surface acidity and the local framework structure, multinuclear solid-state NMR spectroscopy was applied [16–28]. Furthermore, DRIFT spectroscopy of CO adsorption was employed for investigating the changes in the properties of Pd nanoparticles induced by varying the support acidity, and finally, the catalytic materials were tested in the chemoselective hydrogenation of acetophenone. We show that fine-tuning of the support acidity in flame-made $Pd/SiO_2–Al_2O_3$ results in acetophenone hydrogenation catalysts with excellent activity and selectivity to carbonyl hydrogenation products.

2. Experimental

2.1. Catalyst preparation

Aluminum(III) acetylacetonate (99%, ABCR), tetraethoxysilane (99%, Fluka), palladium(II) acetylacetonate (Fluka, 98%), acetic acid (analytical grade, Fluka), and methanol (analytical grade, Fluka) were used as received. The experimental set-up used for the flame spray pyrolysis (FSP) has been described in detail elsewhere [1]. In brief, flame-made silica–alumina loaded with 5 wt% Pd nanoparticles (5 wt% Pd/SA) were prepared by dissolving the corresponding amounts of the precursor materials in a 1:1 (vol.%) mixture of acetic acid and methanol. The resulting solution was filtered over a glass filter, pumped through a capillary with 5 mL/min, and nebulized with 5 L/min O_2. The resulting spray was ignited by an annular supporting methane/oxygen flame (1.5/0.9 L/min) resulting in an approximately 6-cm-long flame. Particles were collected on a cooled Whatman GF6 filter (257 mm diameter). A Busch SV 1040C vacuum pump aided in particle recovery. The 5 wt% Pd/SA catalysts with different Si/Al ratio are denoted as Pd/SA-X, where X corresponds to the fraction of Al (Al at% = Al × 100%/(Al + Si)) in the silica–alumina.

2.2. Textural and morphological properties

Nitrogen physisorption isotherms (adsorption–desorption branches) were measured on a Micromeritics ASAP 2000 instrument at 77 K. Samples were outgassed under vacuum at 423 K before measurement. Specific surface areas of the Pd/SAs were determined by N_2 adsorption using the BET method. Scanning transmission electron microscopy (STEM) images, obtained with a high-angle annular dark field (HAADF) detector, showed the metal particles with bright contrast (Z contrast). In the STEM image, certain areas were selected for a qualitative analysis by energy dispersive X-ray spectroscopy (EDXS; detector (EDAX) attached to the Tecnai F30 microscope (FEI, field emission gun operated at 300 kV)). The ex situ reduced sample was dispersed in ethanol, and some droplets were deposited on a holey carbon foil.

2.3. Solid-state NMR

All catalysts have been pretreated before the NMR investigations. The catalysts were heated under flowing nitrogen at 200 °C during 30 min, followed by reduction in flowing hydrogen for 60 min at the same temperature, and finally cooled down in hydrogen for 30 min. Subsequently, the freshly reduced catalysts were purged with nitrogen for 10 min at room temperature to remove excess hydrogen. Prior to NMR measurements, Pd/SAs were further dehydrated at 400 °C in vacuum at a pressure $p < 10^{-2}$ mbar for 4 h. Afterward, the samples were sealed or used for *in situ* loading. Acetone-2-^{13}C (99.5% ^{13}C-enriched) was purchased from Sigma–Aldrich. To avoid acetone dissociation on Pd nanoparticles, the reduced Pd/SAs were exposed to air for 10 min to allow surface oxidation before dehydration at 400 °C. The dehydrated FSP Pd/SAs were loaded with a surplus of NH_3 and $CH_3{}^{13}COCH_3$ and, subsequently, evacuated at 373 K and room temperature, respectively, for removing weakly hydrogen-bonded or physisorbed compounds. Samples were filled into the MAS NMR rotors in a glove box under dry nitrogen gas.

^{1}H and ^{13}C MAS NMR studies were performed on a Bruker Avance III 400 WB spectrometer at resonance frequencies of 400.1 and 100.4 MHz using 4- and 7-mm probes with spinning rates of ca. 8.0 and 4.0–5.0 kHz, respectively. Spectra were recorded with single-pulse $\pi/2$ excitation and with repetition times of 10 s and 30 s for ^{1}H and ^{13}C nuclei, respectively. Quantitative ^{1}H MAS NMR measurements were performed using an external intensity standard (35% ion-exchanged zeolite H, Na–Y). ^{27}Al MAS NMR investigations were carried out on a Bruker Avance 500 spectrometer at the resonance frequency of 130.3 MHz with a 4-mm Bruker MAS probe and a sample spinning rate of ca. 14 kHz. Single-pulse $\pi/6$ excitation and the repetition time of 500 ms were utilized for the fully hydrated samples. ^{29}Si MAS NMR investigations were carried out on a Bruker AMX 400 spectrometer at a resonance frequency of 79.5 MHz with a 7-mm Bruker MAS probe at a sample spinning rate of ca. 5 kHz. For ^{29}Si MAS NMR, a single-pulse $\pi/2$ excitation with a repetition time of 30 s was applied. To separate the different signals and for the quantitative evaluation of spectra, the data were processed using the Bruker software WINNMR, XWINNMR, and WINFIT.

2.4. Diffuse reflectance infrared Fourier transform spectroscopy

Diffuse reflectance infrared Fourier transform spectroscopy (DRIFTS) combined with CO adsorption was used to gain some insight into the properties of the supported Pd nanoparticles. The investigations were carried out at 297 K with an EQUINOX 55 spectrometer (Bruker Optics) equipped with a liquid nitrogen-cooled HgCdTe detector [9]. The catalyst was introduced into a plug-flow DRIFTS cell and pretreated at 200 °C in a flowing (40 mL/min) mixture of 20 vol.% H_2 in He before CO adsorption. CO adsorption was carried out by flowing a mixture of 10 vol.% CO in He (40 mL/min) over the catalyst for 1 h and then switching to He (40 mL/min) till steady state was achieved. *In situ* IR spectra were collected by averaging 200 scans at 4 cm^{-1} resolution.

2.5. Catalytic hydrogenation

Prior to catalytic tests, the Pd-containing catalysts were reduced using the method as described in the NMR Section 2.3. After purging by nitrogen for 10 min at room temperature, the catalysts were immediately transferred into the stainless steel autoclave (25 mL volume). Before starting the reaction, the autoclave was purged three times with nitrogen and subsequently three times with hydrogen. The reactions were carried out at 50 bar in the autoclave with auto-heating controller and a magnetic stirrer. The autoclave

was equipped with a valve for sample collection; 100 mg of the Pd/SA catalysts and 10 mL acetophenone were stirred magnetically (1000 rpm) at the specified reaction temperatures. The conversion and composition of product mixture were analyzed using a Termo Quest Trace 2000 gas chromatograph equipped with a HP-FFAP (Agilent HP-FFAP 30 m × 0.32 mm × 0.25 μm) capillary column. Bicyclohexyl was used as an internal standard (0.1 mmol). The selectivity to specific product(s) i (S_i) was calculated as S_i (%) = 100 × (i)/[$(APh)_0$ − (APh)], where (i) is the molar concentration of the product(s) and $(APh)_0$ and (APh) correspond to the molar concentration of acetophenone before and after reaction, respectively.

3. Results and discussion

3.1. Textural and morphological properties

BET surface areas of Pd/SAs, determined by N_2 adsorption, were between 174 and 366 m^2/g as summarized in Table 1. This range of surface areas is similar to that of flame-made pure silica–aluminas (FSP SAs) [6], indicating that the loading of silica–aluminas (SAs) with Pd nanoparticles virtually did not influence the specific surface areas. It should be also noted that the surface areas of Pd/SAs increased with the silicon content, as previously observed for pure SAs. The amorphous silica–alumina networks were made up of 4-coordinated silicon and aluminum atoms (dominating ^{27}Al NMR signal at 60 ppm). The Pd nanoparticles in the Pd/SA samples were located predominantly on the outer surface. Note, however, that depending on the conditions of the flame synthesis, incorporation of some Pd into the bulk material cannot be ruled out, as previously observed for other flame-derived supported palladium catalysts [29,30].

STEM images of the Pd/SAs are shown in Fig. 1. The 5 wt% Pd/SA-0 (no Al) catalyst (Fig. 1a) contained Pd nanoparticles with a narrow size distribution in the range of 1–2 nm. When adding aluminum precursor to the feed of the flame affording Pd/SA-15, 30, and 70, the average Pd particle size increased to 3–6 nm (Figs. 1b–d). In contrast to Pt/SAs [4], for Pd/SA, change in the silicon content had less influence on Pd particle size. In addition, the particle shape of these Pd/SA catalysts was virtually not altered by changes in the Si/Al ratio. EDX investigations (two representative examples are shown in Fig. 1e and f) confirmed that the Si/Al ratio of the catalysts was similar to the ratio of the precursors used in the synthesis. Pd dispersions of all alumina containing catalysts were similar and in the range 0.2–0.35, while that of Pd/SA-0 amounted to 0.45, as derived from TEM analysis.

3.2. Acidity and local structure

The acidity and local structure of the Pd/SA catalysts were investigated by multinuclear MAS NMR spectroscopy. Firstly, ^1H MAS NMR spectroscopy was utilized to investigate surface acidity of Pd/SAs. As shown in Fig. 2a bottom, a narrow signal at 1.8 ppm and a shoulder at 2.6 ppm are assigned to silanol groups and hydrogen-bonded silanols of Pd/SA-0. This spectrum is similar to that of the flame-made pure silica. Mostly, Q^3 silicon species ($Si(OSi)_3OH$) and few Q^2 silicon species ($Si(OSi)_2(OH)_2$) are responsible for silanol groups. As shown in Fig. 3a, the strong ^{29}Si MAS NMR signals at −110 and −101 ppm are attributed to the dominating Q^4 silicon species ($Si(OSi)_4$) and Q^3 silicon species ($Si(OSi)_3OH$), respectively. The weak peak at −90 ppm is due to Q^2 silicon species ($Si(OSi)_2(OH)_2$). The silanol groups of Q^3 silicon species have a higher acid strength than those of Q^2 silicon species. However, the molar fraction of hydrogen-bonded silanols at 2.6 ppm on Pd/SA-0 is lower than that of the flame-made pure silica studied in our previous work (Fig. 1a in Ref. [6]). This finding indicates that some Pd nanoparticles are located in the vicinity of SiOH groups and block interactions with neighboring silanols. After adsorption of ammonia on Pd/SA-0 and subsequent evacuation at 373 K, no formation of ammonium ions (signal at ca. 7 ppm) caused by Brønsted acid sites was observed in the ^1H MAS NMR spectrum (Fig. 2a, top).

When adding aluminum precursor to the flame feed, the hydrogen bondings between silanol groups decreased as indicated by a significant decrease in the shoulder at 2.6 ppm in the ^1H MAS NMR spectra in Fig. 2b–d. This is attributed to the incorporation of the aluminum atoms in the vicinity of SiOH groups that block the interaction between them as also discussed for Pd nanoparticles. This behavior is further confirmed by ^{29}Si and ^{27}Al MAS NMR investigations. As shown in Fig. 3, increasing the aluminum content results in a low-field shift of the ^{29}Si NMR signals of the main peaks (from −110 ppm to −90 ppm), which indicates a substitution of silicon sites by aluminum atoms. The ^{27}Al MAS NMR spectrum of Pd/SA-15 in Fig. 4a shows that most aluminum species are 4-coordinated (60 ppm) inside the silica network, e.g., as $Al(OHSi)(OSi)_3$ species. Therefore, the acid strength of silanol groups is enhanced by neighboring aluminum atoms.

Adsorption of basic probe molecules is well established to distinguish between non-acidic and acidic surface sites. As shown in our recent work [6], adsorption of NH_3 and subsequent evacuation of the samples at 373 K allow the assignment of Brønsted acid sites of SAs, which are able to protonate NH_3 to form ammonium ions (7.0 ppm in ^1H MAS NMR spectra). These ammonium ions possess a high thermal stability and can be utilized for quantifying the number of Brønsted acid sites. As shown in Fig. 2, the ^1H NMR signals of ammonium ions at 7 ppm were observed for all Pd/SAs catalysts with aluminum contents of 15–70 at%. It indicates that the presence of aluminum atoms in the supports obviously enhances the acidity of these materials. Evaluation of the intensity of the signal at 7 ppm allowed determining the concentration and molar fraction of these Brønsted acid sites (see Table 1, second and third column).

As shown in Fig. 2, the intensity of the peak at ca. 7 ppm increased with increasing aluminum content from 15% to 70%. Therefore, the concentrations of Brønsted acid sites of Pd/SAs can be tuned by varying the aluminum content as previously described [6]. As shown in Table 1, the concentration and molar fraction of the Brønsted acid sites increase with the aluminum content up to 70%. In our previous study, on flame-made silica–alumina, we

Table 1
Properties of flame-made Pd/silica–alumina (Pd/SA) catalysts. BET surface areas, concentrations of Brønsted acid sites, and fractions of aluminum species with different oxygen coordination.

Pd/SAs	Surface area (m^2/g)	Brønsted acidic OH (mmol/g)	Brønsted acidic OH (mol%)*	Al^{IV} (at%)	Al^{V} (at%)	Al^{VI} (at%)
Pd/SA-0	366	–	–	–	–	–
Pd/SA-15	299	7.9×10^{-2}	7.5	69.1	9.8	21.2
Pd/SA-30	210	8.8×10^{-2}	8.6	50.7	26.3	23.0
Pd/SA-70	174	10.3×10^{-2}	12.8	37.3	35.3	27.4

* Brønsted acidic OH (mol%) = (number of Brønsted acidic OH groups/total number of OH groups on supports)×100%.

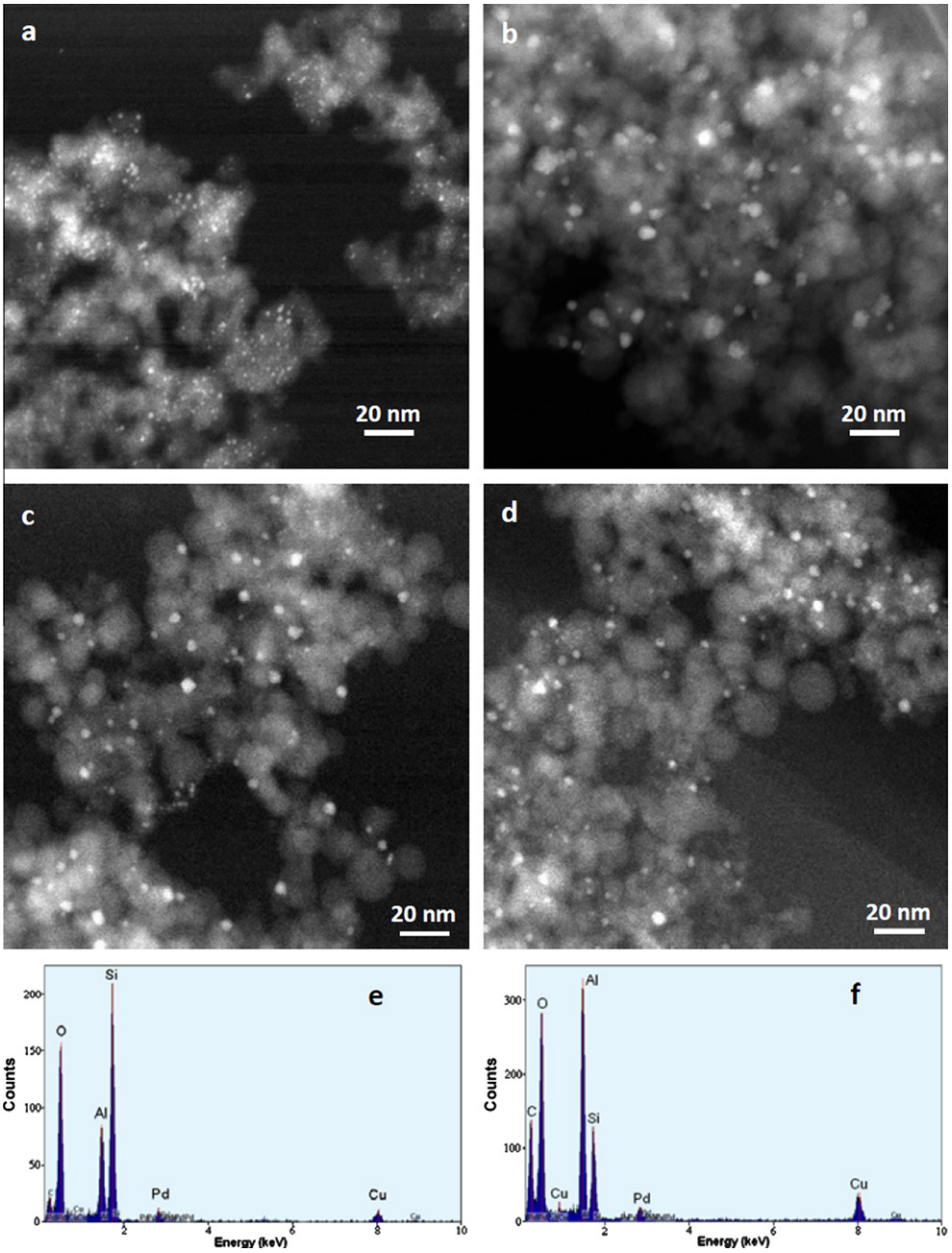

Fig. 1. STEM images of the Pd/silica–alumina catalysts: Pd/SA-0 (a), Pd/SA-15 (b), Pd/SA-30 (c), and Pd/SA-70 (d) catalyst. EDX spectra of Pd/SA-30 (e) and Pd/SA-70 (f).

found that the penta-coordinated aluminum (Al^V) species can strongly influence the nearby silanols and enhance their Brønsted acidity. Fig. 4 shows that the intensity of the ^{27}Al MAS NMR signal at 35 ppm due to Al^V species is increasing from Pd/SA-15 with 15 at% aluminum to Pd/SA-70 with 70 at% aluminum. Based on the quantitative evaluation of ^{27}Al MAS NMR spectra, the molar fractions of three aluminum species (Al^{IV}, Al^V, and Al^{VI}) on Pd/SAs were estimated (Table 1). The fraction of Al^V increased with increasing molar fraction of Brønsted acid sites. However, the concentration of Brønsted acid sites on Pd/SAs is obviously lower than that on previously made pure silica–alumina (8.8×10^{-2} for Pd/SA-30, 11.1×10^{-2} for SA-30; 10.3×10^{-2} for Pd/SA-70, 15.1×10^{-2} for SA-70). This is attributed to some covering (blocking) of these surface sites on Pd/SAs by Pd particles.

We applied the adsorption of acetone ($CH_3^{13}COCH_3$) to study the strength of the Brønsted acid sites formed in the Pd/SA materials. This probe molecule is widely used for distinguishing surface OH groups with different acid strengths. The adsorbate-induced low-field shift ($\Delta\delta_{13C}$) of acetone upon interaction with solid acids is a well-accepted scale for acid strength [27]. Fig. 5 shows ^{13}C MAS NMR spectra of pretreated Pd/SAs recorded after loading samples with acetone-2-^{13}C. Acetone-2-^{13}C adsorbed on Brønsted acid sites of Pd/SA-15 and Pd/SA-30 gave rise to a signal at 213 ppm, while the ^{13}C MAS NMR spectrum of acetone-loaded Pd/SA-70 was dominated by peaks at 215 ppm. For Pd/SAs with aluminum contents higher than 30%, there were no signals at resonance positions corresponding to Brønsted acid sites of zeolites (216–223 ppm). However, comparison of the ^{13}C MAS NMR spectra of the

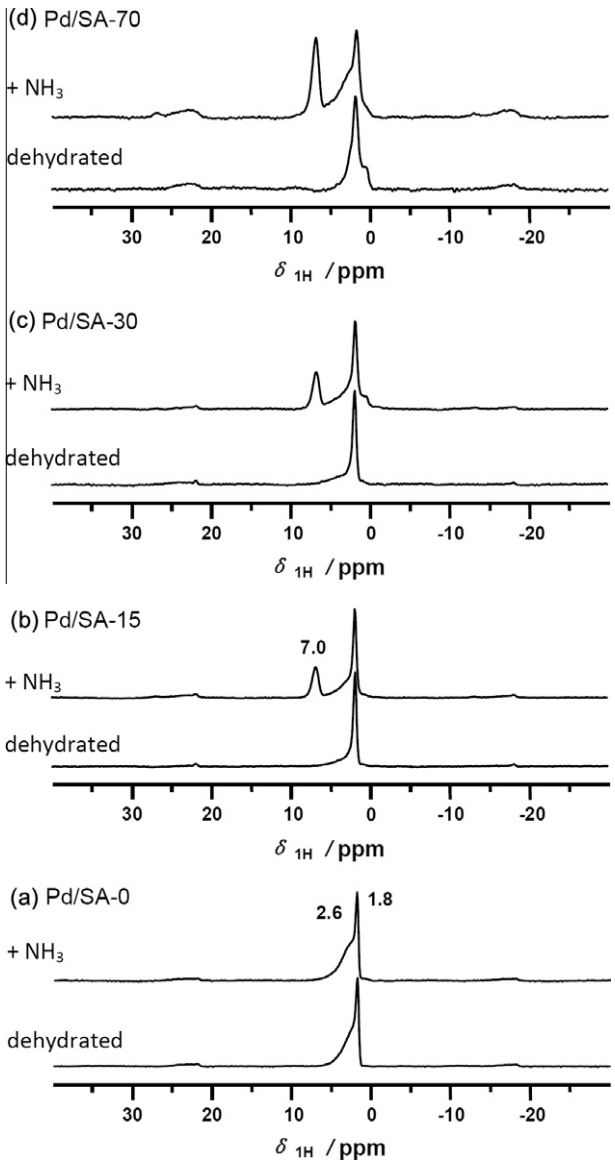

Fig. 2. ^{1}H MAS NMR spectra of pretreated Pd/SA-0 (a), Pd/SA-15 (b), Pd/SA-30 (c), and Pd/SA-70 (d) recorded before and after loading with NH_3 and subsequent evacuation at 373 K for 1 h.

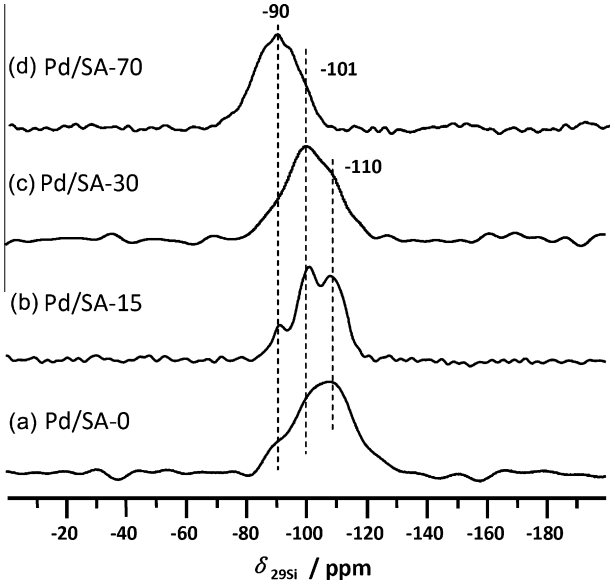

Fig. 3. ^{29}Si MAS NMR spectra of Pd/SA-0 (a), Pd/SA-15 (b), Pd/SA-30 (c), and Pd/SA-70 (d).

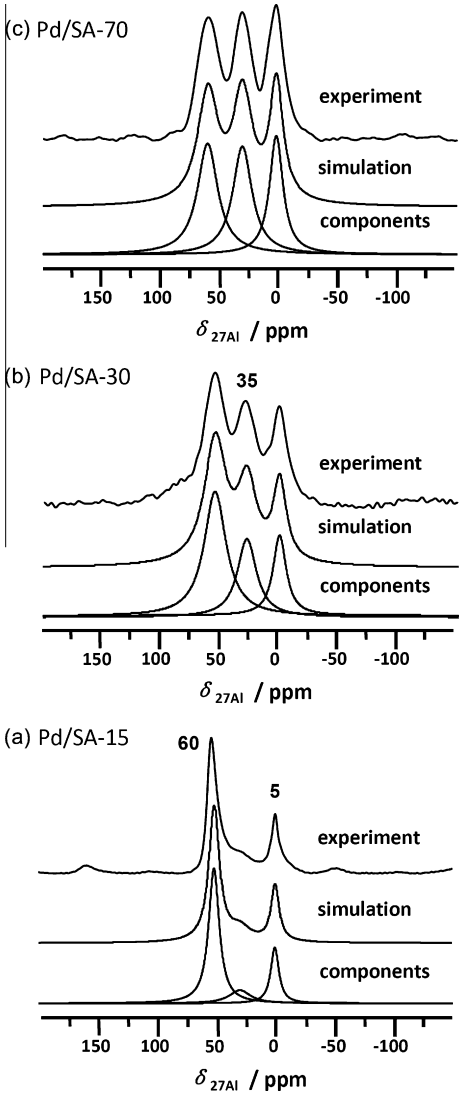

Fig. 4. ^{27}Al MAS NMR spectra of Pd/SA-15 (a), Pd/SA-30 (b), and Pd/SA-70 (c).

acetone-loaded Pd/SAs under study showed a low-field shift of the acetone signal for the materials with higher aluminum contents. This finding indicates an enhanced strength of the Brønsted acid sites of Pd/SA-70 compared to corresponding Pd/SA materials with low aluminum contents.

It is well known that the formation of Brønsted acid sites on amorphous silica–alumina is related to the local structure of silanol groups. Therefore, we propose that the introduction of Pd during flame synthesis leading to incorporation of these metal atoms into the local structure of the SiOH groups causes a change in the acid strength of these materials. In amorphous silica–alumina, the Brønsted acidity is generated by silanols, which are strongly influenced by neighboring aluminum [31]. When one aluminum is incorporated in the vicinity of a silanol group, this surface OH group becomes a Brønsted acid site. For flame-made silica–alumina with a high aluminum content, such as SA-70, a large number of aluminum atoms are incorporated into the silica framework and the local structure of the silanol groups affording many Brønsted acidic silanol groups with enhanced acid strength. However, these

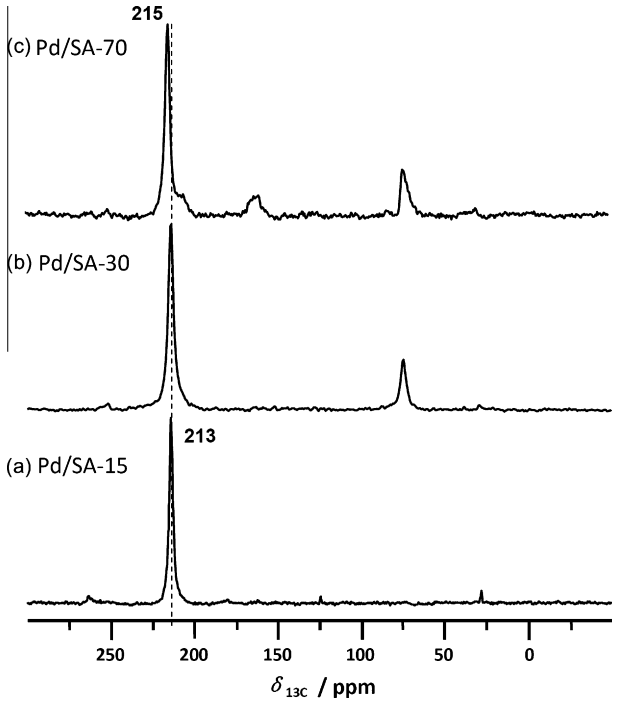

Fig. 5. ^{13}C MAS NMR spectra of pretreated Pd/SA-15 (a); Pd/SA-30 (b); and Pd/SA-70 (c) recorded after loading and evacuation of acetone-2-^{13}C ($CH_3^{13}COCH_3$).

enhanced Brønsted acid sites were not detected with Pd/SA-70, though its structure shows similar aluminum coordination as the non-metal-loaded SA-70. Penta-coordinated aluminum is an interface species between alumina and a mixed silica–alumina phase or between an alumina-type phase and a mixed silica–alumina phase [32]. Al^V species can exist in the vicinity to silicon in part of the alumina network. The 'pseudo-bridging' was generated between Al^V and Brønsted acid sites and caused a transfer of electron density from OH groups, which further increases the acid strength of these sites on SA-70 [33]. Introduction of Pd particles on silica–alumina during flame synthesis occurred preferentially around silanols as indicated by the ^1H MAS NMR investigation. Therefore, the 'pseudo-bridging' between Al^V and Brønsted acid sites might be blocked, and the acidity of these sites cannot be further enhanced.

The signal at ca. 75 ppm in Fig. 5b is due to the formation of diacetone alcohol on Pd/SA-30, and the additional weak peak at ca. 170 ppm in Fig. 5c is attributed to the formation of mesityl oxide on Pd/SA-70. Increasing the aluminum content in the FSP synthesis likely resulted in the formation of an alumina phase on the surface of some particles, generating Lewis acid sites. Alumina with Lewis acidity was detected to initiate acid-catalyzed condensation immediately after adsorption of acetone [34]. Therefore, the adsorption of acetone on the alumina phase of Pd/SA-30 caused a condensation reaction affording diacetone alcohol. Pd/SA-70 with the highest alumina content also catalyzed the further reaction generating a small amount of mesityl oxide.

3.3. DRIFT spectroscopy of adsorbed CO

Infrared spectroscopy of CO adsorbed on supported noble metal clusters is widely used to gain some insight into structural and electronic properties of nanoparticles. In addition, the catalytic performance of supported metal particles can be also influenced by the electronic interaction between metal and acid-basic groups on the oxide supports [35]. There are mainly two regions of bands that can be distinguished for adsorbed CO: bands at higher wavenumbers (2050–2150 cm^{-1}) due to linearly coordinated CO and bands at lower wavenumbers (1900–2000 cm^{-1}) assigned to CO adsorbed in bridged coordination. In addition, the positions of the bands depend on particle size, surface coverage, and electronic changes due to different metal structures [36]. Fig. 6 shows the DRIFT spectra of CO adsorbed on the reduced Pd/SA-15 and Pd/SA-70. The bands around 2090–2100 cm^{-1} in both spectra are assigned to linearly coordinated CO on (1 1 1) and (1 0 0) terraces of highly coordinated Pd atoms [37]. The weak band at ca. 2070 cm^{-1} is due to linearly coordinated CO adsorbed on low coordinated Pd sites at step edges, corners, and defects [37]. As described in the last section, the acid strength of the SA support of the Pd/SA-70 catalyst is higher than that of Pd/SA-15. The intensity of the band corresponding to linearly coordinated CO on Pd(1 1 1) and Pd(1 0 0) terraces is enhanced and shifted from 2092 cm^{-1} to 2100 cm^{-1} with increasing acid strength (Figs. 6a and b).

The bands between 1900 and 2000 cm^{-1} in the DRIFT spectra are attributed to bridged CO on supported Pd nanoparticles. For Pd/SA-15, a band appeared at 1970 cm^{-1}, i.e., between 1948 and 1990 cm^{-1}. This band is assigned to bridged CO on the edges of Pd aggregates with Pd(1 1 1) facets [38]. Freund and coworkers proposed that the larger Pd aggregates grow during synthesis with shapes defined by cubo-octahedra [38]. The ratio of Pd(1 0 0) to Pd(1 1 1) facets for cubo-octahedra of a size of ca. 5 nm would be approximately 1:5. Reversely, this band at 1970 cm^{-1} disappeared in the DRIFT spectrum of Pd/SA-70. It may indicate that the smaller Pd aggregates grown during flame synthesis were less ordered. The bands at 1990 and 1948 cm^{-1} in both spectra are attributed to bridged CO on Pd terraces.

According to theoretical and experimental investigations, the intensity ratio of bridged to linearly (B/L) coordinated CO is a crucial parameter for the electronic properties of supported transition metals [36,39–43]. As emerges from Fig. 6, the B/L ratio decreases with increasing acidity of the SA support of Pd/SA-70. The lower B/L ratio indicates a decrease in electron density on the supported Pd nanoparticles. With increasing support acidity, the electronic charge of the support oxygen atoms decreases, which further

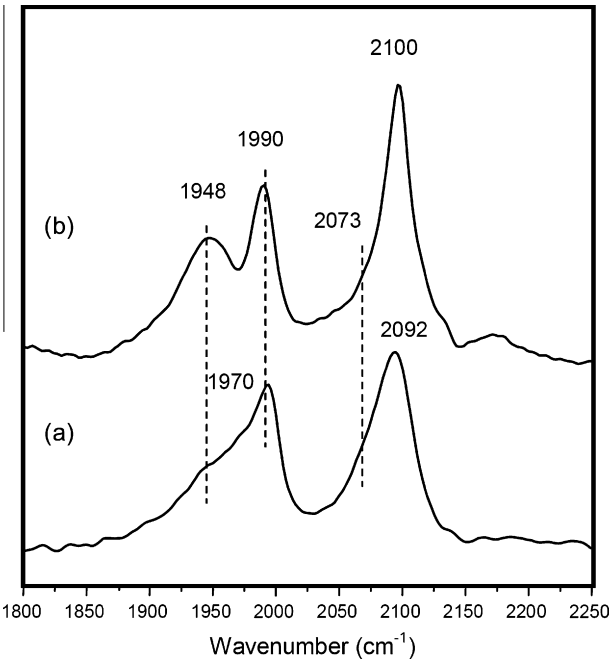

Fig. 6. DRIFT spectra of CO adsorption on reduced Pd/SA-15 (a) and Pd/SA-70 (b).

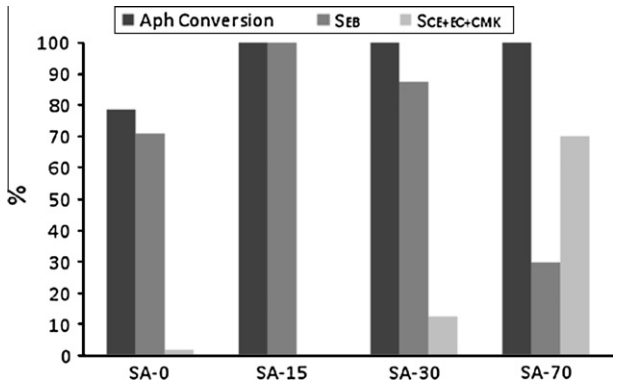

Fig. 7. Conversion of APh and selectivity to products (S_{EB}, selectivity to CO bond hydrogenolysis to produce EB, and $S_{CE+EC+CMK}$, selectivity to phenyl ring hydrogenation products affording (CE + EC + CMK) for the hydrogenation of APh on Pd/SA-0, Pd/SA-15, Pd/SA-30, and Pd/SA-70. Note that with Pd/SA-15 no hydrogenation of the aromatic ring occurred even when the reaction time was extended from 3 h to 4 h. Standard conditions: 170 °C, 50 bar hydrogen pressure, 3 h reaction time.

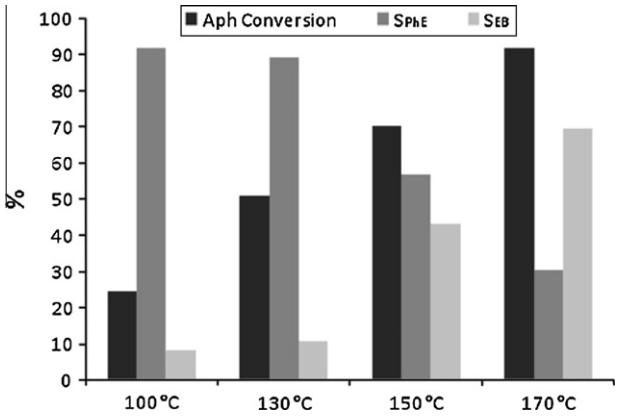

Fig. 8. Conversion of APh and selectivity to PhE (S_{PhE}) and EB (S_{EB}) for hydrogenolysis of APh C=O bond on Pd/SA-15 catalyst at various temperatures. Conditions: 50 bar hydrogen pressure, 2 h reaction time.

decreases the electron density on the supported Pd nanoparticles [42,43].

3.4. Chemoselective hydrogenation of acetophenone

As discussed above, tuning the Si/Al ratio of the SA changed the acidity of these materials, which in turn influenced the electronic properties of the supported Pd nanoparticles. Differences in hydrogen chemisorption properties caused by changes in the electron densities of the transition metal nanoparticles are reflected in the different catalytic activity of these particles in hydrogenation and hydrogenolysis reactions [10]. In order to study these effects, we applied the chemoselective hydrogenation of acetophenone (Aph) as a test reaction. Scheme 1 shows the possible reaction pathways of this hydrogenation reaction [44,45]. The selective hydrogenation of the carbonyl group affords 1-phenylethanol (PhE) and ethylbenzene (EB). Cyclohexylmethylketone (CMK) is the primary product resulting from the hydrogenation of the aromatic ring. In consecutive steps, this primary product can be converted to 1-cyclohexylethanol (CE) and ethylcyclohexane (EC). Recently, it has been shown that 1-cyclohexylethanol cannot be directly converted to ethylcyclohexane (EC) by hydrogenolysis of the C—OH bond [4].

Hydrogenation of acetophenone (Aph) was studied on Pd/SA-0, Pd/SA-15, Pd/SA-30, and Pd/SA-70 in an autoclave at a hydrogen pressure of 50 bar. In Fig. 7, the conversion of APh and selectivities (S_{EB} and $S_{CE+EC+CMK}$) to the different products resulting at 170 °C after 3 h reaction time are presented. The conversion of APh was 78% on Pd/SA-0 and reached 100% for Pd/SA-15, Pd/SA-30, and Pd/SA-70. The main products on Pd/SA-0 were EB (selectivity of 70.7%) and PhE (selectivity of 27.1%). However, the primary product of the Aph hydrogenation was PhE rather than EB on Pd/SA-0 at 80 °C after 30 min (not shown). There was no EB observed under these reaction conditions. Based on TPD and IR investigations, the adsorption geometry of Aph on Pd/SiO_2 was proposed to assume a η^2(C,O) configuration, that is, the carbonyl group coordinates by means of the π-electrons of C=O and the tilted phenyl group bonded to the Pd surface [46]. It promotes both C and O atoms of the carbonyl group interacting with chemisorbed H on the Pd surface to form PhE.

For Pd/SA-15, where Brønsted acid sites were present on the support, nearly all Aph molecules were converted to EB as shown schematically in Fig. 7. The TOFs (at 170 °C) related to the number

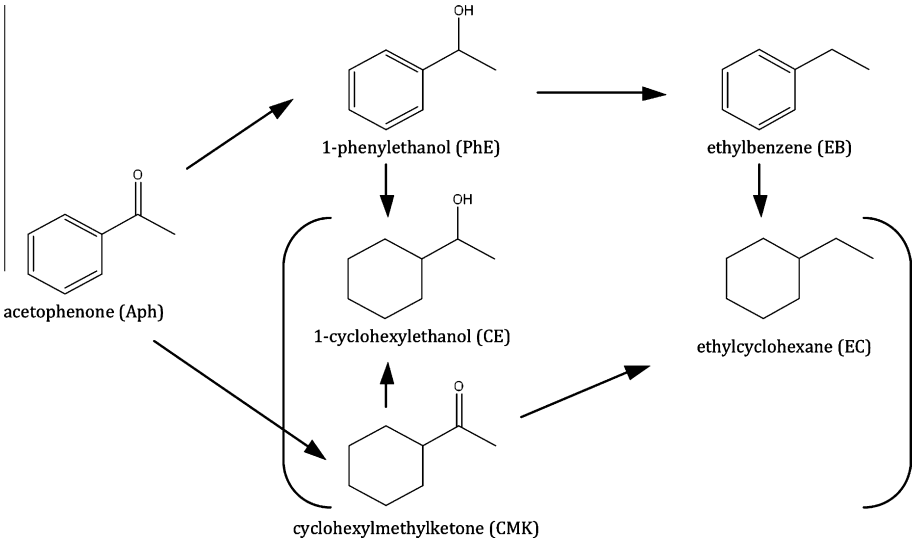

Scheme 1.

of surface Pd atoms were 0.43 s^{-1} for Pd/SA-0, 0.76 s^{-1} for Pd/SA-15, 0.78 s^{-1} for Pd/SA-30, and 0.85 s^{-1} for Pd/SA-70. Although a direct comparison of the activity of the catalysts with other catalysts reported in the literature [4,12–15] is difficult due to the fact that different conditions (temperature, solvent, etc.) were used, we can still conclude that the flame-derived catalysts are among those possessing the highest activity. Interestingly, comparison with our previously reported flame-derived Pt/SA catalysts reveals that Pd/SAs tested here in the solvent-free hydrogenation of Aph seem to be more active than Pt/SAS in the same reaction with organic solvents (TOFs at 20 °C in the range of 0.13–0.22 s^{-1}) [4]. Obviously, enhancement of the support acidity increases the activity of both flame-derived Pd/SA as well as Pt/SA catalysts [4] for hydrogenation of Aph. It is widely accepted that introducing acidic solvents or acidic supports can promote catalytic hydrogenation on transition metals [47,48]. At the same time, the catalysts with acidic supports always show bifunctional catalytic properties. Increase in the support acidity reduces the adsorption energy of hydrogen on the supported metal nanoparticles [10], which in turn enhances the activity of the catalyst in hydrogenation reactions. The Brønsted acid sites promote the Aph hydrogenation. In the hydrogenation of Aph on Ni–Pt/zeolite Y catalysts in alcoholic solvents (MeOH, EtOH, and isopropanol), little styrene and large amounts of relevant ether derivatives were produced [45]. The acidic sites on the supports led to the catalytic dehydration of the primary product PhE affording styrene or initiated the etherification with alcohols to generate ether derivatives. Then, the C=C bond of styrene was fastly hydrogenated to EB.

In our solvent-free hydrogenation, no styrene was detected, which is reasonable because styrene is only produced in polar protic solvents. These solvents can stabilize carbocations of secondary alcohol derivatives for further dehydration during the reaction [45]. In the present work, the Brønsted acid sites on the supports of the Pd/SAs are also proposed to activate the C—OH groups of PhE due to their strong electron donor property, which should promote their interaction with dissociated hydrogen. It should be mentioned that zeolite Y has Brønsted acid sites, which have an acid strength corresponding to a ^{13}C MAS NMR shift of adsorbed acetone-2-^{13}C of 220 ppm. Hence, the above-mentioned sites are significantly stronger than the Brønsted acid sites on the supports of the Pd/SAs materials (acetone-2-^{13}C signal at 213–215 ppm, see Fig. 5) [49]. This may affect the selectivity to EB, which is lower than 10% for the Aph hydrogenation on Pd/SAs at 100 °C after 2 h (Pd/SA-15 see Fig. 8; Pd/SA-30 and Pd/SA-70 not shown). However, increasing the reaction temperature can also enhance the catalyst activity, which may also contribute to the enhanced EB selectivity on Pd/SA-15 at temperatures higher than 150 °C.

Interestingly, Pd/SA-15 showed a high chemoselectivity to the carbonyl group during hydrogenation of Aph. Nearly no formation of CE, EC, and CMK was observed. Irrespective of the degree of Aph conversion, the selectivity toward EB and PhE (S_{EB+PhE}) was 100% for Pd/SA-15, as shown in Fig. 8. With increase in the reaction temperature from 100 to 170 °C, the conversion of APh increased from 24.8% to 90.2% along with the selectivity to EB that increased from 8.3% to 69.5%, confirming a highly selective consecutive pathway from Aph via PhE to EB. Strikingly, after all Aph had been converted to EB at 170 °C, extending the reaction time (3 h) by another 30 min or 1 h did not cause further hydrogenation of aromatic rings to EC.

Further enhancement of the support acidity (Pd/SA-30 and Pd/SA-70) resulted in higher rates (see TOFs given above) and hydrogenation of the aromatic ring, decreasing the selectivity S_{EB+PhE} from 89.3% for Pd/SA-30 to 58.6% for Pd/SA-70 at 80% conversion of Aph. On Pd/SA-70, both hydrogenolysis of carbonyl groups and hydrogenation of aromatic rings occurred in 10 min at 170 °C. It is assumed that further enhanced support acidity strongly increases the hydrogen dissociation on the Pd surface and enhances the hydrogenation activity of the catalysts. In addition, we proposed that the acid sites in the vicinity of the Pd nanoparticles also affect the catalytic properties of Pd/SA-70. In a previous study [50], it was found that the activation energy for the protonation of the aromatic rings is related to the Brønsted acidity: The presence of Brønsted acid sites lead to a lower activation energy. In addition, Pd nanoparticles were located close to the Brønsted acid sites as indicated by MAS NMR investigations of Pd/SA-70, which may promote the interaction between active hydrogen and activated aromatic rings in the hydrogenation reaction.

Finally, the reusability of the most selective catalyst Pd/SA-15 was investigated. For this purpose, the used Pd/SA-15 catalyst was filtered and further washed with *n*-hexane as solvent [4]. After drying under vacuum overnight at 30 °C, the catalyst was reused in the hydrogenation reaction of the same amount of reactant at 170 °C and 50 bar. The activity and selectivity of the reused Pd/SA-15 remained virtually the same, and no hydrogenation of aromatic ring was observed.

4. Conclusions

A single-step synthesis method, flame spray pyrolysis, was applied to prepare silica–alumina–supported Pd nanoparticle (Pd/SA) catalysts for the solvent-free hydrogenation of an aromatic ketone (acetophenone). The acidity of the silica–alumina support could be easily tuned by changing the Si/Al ratio in the precursor solutions fed to the flame. Quantitative ^{1}H MAS NMR investigations, combined with adsorption of NH_3 as probe molecule, showed that Pd/SA-0 (no Al) only contained non-acidic silanol groups. The Pd nanoparticles on the pure silica support (SA-0) were located in the vicinity of SiOH groups and blocked interactions between the silanol groups. Adding aluminum in the precursor solutions used in the flame synthesis, afforded Brønsted acid sites on SA-15, SA-30, and SA-70 due to aluminum atoms in the vicinity of SiOH groups. The concentration of Brønsted acid sites increased with the aluminum content up to 70 at%. Brønsted sites with enhanced acid strength in the Pd/SAs with higher aluminum contents, which were loaded with acetone-2-^{13}C as probe molecules, showed narrow ^{13}C MAS NMR signals at 213–215 ppm (compared with 220 and 223 ppm for zeolites H–Y and H–ZSM-5, respectively).

Quantitative ^{1}H MAS NMR spectroscopy indicated that 2.3×10^{-2} mmol/g and 3.8×10^{-2} mmol/g Brønsted acid sites were covered by Pd nanoparticles on Pd/SA-30 and Pd/SA-70, respectively. The electronic properties of the supported Pd nanoparticles changed as a result of the tuning of the support acidity. The intensity ratio of bridged to linear (B/L) bonded CO, as determined by DRIFT spectroscopy, decreased with increasing support acidity, indicating a decrease in the electron density on the supported Pd nanoparticles. This is assumed to reduce the adsorption strength of hydrogen on Pd/SAs and to lead to an increase in the hydrogenation activity of the catalysts. In fact, the increase in the support acidity from Pd/SA-0 to Pd/SA-15 afforded higher reaction rate (TOF) and outstanding chemoselectivity to carbonyl group hydrogenation of acetophenone, all APh was converted to ethylbenzene (99.9%) and 1-phenylethanol (0.1%) at 170 °C, even at prolonged reaction times. Further enhancement of the support acidity as achieved in Pd/SA-30 and Pd/SA-70 further increased the reaction rate and promoted the competing hydrogenation of the aromatic ring.

In conclusion, the Pd/silica–alumina catalysts prepared by single-step flame spray pyrolysis give access to easy tunability of the support acidity and show interesting catalytic properties for the chemoselective hydrogenation of acetophenone under solvent-free conditions. Extension of the application of these catalysts

to chemoselective hydrogenation of other aromatic ketones as well as to other reactions seems promising.

Acknowledgments

We greatly appreciated the financial support by ETH Zürich (TH-09 06-2). We thank Dr. Frank Krumeich (ETH) for the STEM/EDXS investigations. Electron microscopy was performed at EMEZ (Electron Microscopy, ETH Zürich).

References

[1] R. Strobel, A. Baiker, S.E. Pratsinis, Adv. Powder Technol. 17 (2006) 457.
[2] B. Schimmoeller, Y.J. Jiang, S.E. Pratsinis, A. Baiker, J. Catal. 274 (2010) 64.
[3] S. Roy, N. van Vegten, A. Baiker, J. Catal. 271 (2010) 125.
[4] B. Schimmoeller, F. Hoxha, T. Mallat, F. Krumeich, S.E. Pratsinis, A. Baiker, Appl. Catal. A 374 (2010) 48.
[5] E. Schmidt, F. Hoxha, T. Mallat, A. Baiker, J. Catal. 274 (2010) 117.
[6] J. Huang, N. van Vegten, Y.J. Jiang, M. Hunger, A. Baiker, Angew. Chem. Int. Ed. 49 (2010) 7776.
[7] G.W. Huber, S. Iborra, A. Corma, Chem. Rev. 106 (2006) 4044.
[8] G. Ertl, H. Knözinger, F. Schüth, J. Weitkamp, Handbook of Heterogeneous Catalysis, second ed., Wiley-VCH, Weinheim, Germany, 2008.
[9] F. Hoxha, B. Schimmoeller, Z. Cakl, A. Urakawa, T. Mallat, S.E. Pratsinis, A. Baiker, J. Catal. 271 (2010) 115.
[10] M.K. Oudenhuijzen, J.A. van Bokhoven, J.T. Miller, D.E. Ramaker, D.C. Koningsberger, J. Am. Chem. Soc. 127 (2005) 1530.
[11] J. Weitkamp, L. Puppe, Catalysis and Zeolites – Fundamentals and Application, Springer-Verlag, Berlin, 1999.
[12] S. Nishimura, Handbook of Heterogeneous Catalytic Hydrogenation for Organic Synthesis, John Wiley & Sons, New York, 2001.
[13] S.D. Lin, D.K. Sanders, M. Albert Vannice, Appl. Catal. A 113 (1994) 59.
[14] C.-S. Chen, H.-W. Chen, Appl. Catal. A 260 (2004) 207.
[15] F. Jutz, J.M. Andanson, A. Baiker, J. Catal. 268 (2009) 356.
[16] S.H. Li, A.M. Zheng, Y.C. Su, H.L. Zhang, L. Chen, J. Yang, C.H. Ye, F. Deng, J. Am. Chem. Soc. 129 (2007) 11161.
[17] M. Haouas, S. Walspurger, F. Taulelle, J. Sommer, J. Am. Chem. Soc. 126 (2004) 599.
[18] J. Trebosc, J.W. Wiench, S. Huh, V.S.Y. Lin, M. Pruski, J. Am. Chem. Soc. 127 (2005) 3057.
[19] J. Kanellopoulos, C. Gottert, D. Schneider, B. Knorr, D. Prager, H. Ernst, D. Freude, J. Catal. 255 (2008) 68.
[20] J. Weitkamp, M. Hunger, Stud. Surf. Sci. Catal. 168 (2007) 787.
[21] L.M. Peng, C.P. Grey, Micropor. Mesopor. Mater. 116 (2008) 277.
[22] A.G. Stepanov, S.S. Arzurnanov, M.V. Luzgin, H. Ernst, D. Freude, V.N. Parmon, J. Catal. 235 (2005) 221.
[23] A. Simperler, R.G. Bell, M.W. Anderson, J. Phys. Chem. B 108 (2004) 7142.
[24] J.F. Haw, T. Xu, J.B. Nicholas, P.W. Goguen, Nature 389 (1997) 832.
[25] C. Collins, G. Mann, E. Hoppe, T. Duggal, T.L. Barr, J. Klinowski, Phys. Chem. Chem. Phys. 1 (1999) 3685.
[26] E.M. El-Malki, R.A. van Santen, W.M.H. Sachtler, J. Phys. Chem. B 103 (1999) 4611.
[27] C. Paze, A. Zecchina, S. Spera, G. Spano, F. Rivetti, Phys. Chem. Chem. Phys. 2 (2000) 5756.
[28] G. Crepeau, V. Montouillout, A. Vimont, L. Mariey, T. Cseri, F. Mauge, J. Phys. Chem. B 110 (2006) 15172.
[29] N. van Vegten, M. Maciejewski, F. Krumeich, A. Baiker, Appl. Catal. B: Environ. 93 (2009) 38.
[30] S.B. Bubenhofer, F. Krumeich, R. Fuhrer, E.K. Athanassiou, W.J. Stark, R.N. Grass, J. Phys. Chem. C 115 (2011) 1269.
[31] G. Busca, Chem. Rev. 107 (2007) 5366.
[32] M.F. Williams, B. Fonfe, C. Sievers, A. Abraham, J.A. van Bokhoven, A. Jentys, J.A.R. van Veen, J.A. Lercher, J. Catal. 251 (2007) 485.
[33] C. Chizallet, P. Raybaud, Angew. Chem. Int. Ed. 48 (2009) 2891.
[34] A.I. Biaglow, R.J. Gorte, D. White, J. Catal. 150 (1994) 221.
[35] F. Solymosi, Catal. Rev. 1 (1968) 233.
[36] B.L. Mojet, J.T. Miller, D.E. Ramaker, D.C. Koningsberger, J. Catal. 186 (1999) 373.
[37] D. Tessier, A. Rakai, F. Bozonverduraz, J. Chem. Soc., Faraday Trans. 88 (1992) 741.
[38] K. Wolter, O. Seiferth, J. Libuda, H. Kuhlenbeck, M. Baumer, H.J. Freund, Surf. Sci. 404 (1998) 428.
[39] R.A. van Santen, J. Chem. Soc. Faraday Trans. 1 (83) (1987) 1915.
[40] A.Y. Stakheev, Y. Zhang, A.V. Ivanov, G.N. Baeva, D.E. Ramaker, D.C. Koningsberger, J. Phys. Chem. C 111 (2007) 3938.
[41] D.C. Koningsberger, D.E. Ramaker, J.T. Miller, J. de Graaf, B.L. Mojet, Top. Catal. 15 (2001) 35.
[42] T. Visser, T.A. Nijhuis, A.M.J. van der Eerden, K. Jenken, Y.Y. Ji, W. Bras, S. Nikitenko, Y. Ikeda, M. Lepage, B.M. Weckhuysen, J. Phys. Chem. B 109 (2005) 3822.
[43] M. Lepage, T. Visser, A.M.J. van der Eerden, F. Soulimani, B.M. Weckhuysen, Vib. Spectrosc. 48 (2008) 92.
[44] C.S. Chen, H.W. Chen, W.H. Cheng, Appl. Catal. A 248 (2003) 117.
[45] R.V. Malyala, C.V. Rode, M. Arai, S.G. Hegde, R.V. Chaudhari, Appl. Catal. A 193 (2000) 71.
[46] H.W. Chen, C.S. Chen, S.J. Harn, J. Phys. Chem. 99 (1995) 10557.
[47] D.Y. Hong, S.J. Miller, P.K. Agrawal, C.W. Jones, Chem. Commun. 46 (2010) 1038.
[48] C. Zhao, Y. Kou, A.A. Lemonidou, X.B. Li, J.A. Lercher, Angew. Chem. Int. Ed. 48 (2009) 3987.
[49] J.F. Haw, J.B. Nicholas, T. Xu, L.W. Beck, D.B. Ferguson, Acc. Chem. Res. 29 (1996) 259.
[50] J. Huang, Y.J. Jiang, V.R.R. Marthala, W. Wang, B. Sulikowski, M. Hunger, Micropor. Mesopor. Mater. 99 (2007) 86.